2020

From Neutral Aniline to Aniline Trication: A Computational and Experimental Study

G. L. Gutsev
Florida A&M University

H. A. López Peña
Virginia Commonwealth University

S. L. McPherson
Virginia Commonwealth University

See next page for additional authors

From Neutral Aniline to Aniline Trication: A Computational and Experimental Study

G. L. Gutsev,*[a] H. A. López Peña,[b] S. L. McPherson,[b] D. Ampadu Boateng,[b] B. R. Ramachandran,[c] L. G. Gutsev,[c,d] K. M. Tibbetts*[b]

[a] *Department of Physics, Florida A&M University, Tallahassee, Florida 32307, United States*

[b] *Department of Chemistry, Virginia Commonwealth University, Richmond, Virginia 23284, United States*

[c] *Institute for Micromanufacturing, Louisiana Tech University, Ruston, LA 71272, United States*

[d] *Institute of Problems of Chemical Physics of Russian Academy of Sciences, Chernogolovka, Moscow District 142432, Russia*

Abstract

We report density functional theory computations and photoionization mass spectrometry measurements of aniline and its positively charged ions. The geometrical structures and properties of the neutral, singly, doubly, and triply positively charged aniline are computed using density functional theory with the generalized gradient approximation. At each charge, there are multiple isomers closely spaced in total energy. Whereas the lowest energy states of both neutral and cation have the same topology $C_6H_5–NH_2$, the dication and trication have the $C_5NH_5–CH_2$ topology with the nitrogen atom in the meta and para positions, respectively. We compute the dissociation pathways of all four charge states to NH or NH^+ and NH_2 or NH_2^+, depending on the initial charge of the aniline precursor. Dissociation leading to the formation of NH (from the neutral and cation) and NH^+ (from the dication and trication) proceeds through multiple transition states. On the contrary, the dissociation of NH_2 (from the neutral, cation) and NH_2^+ (from the dication and trication) is found to proceed without an activation energy barrier. The trication was found to be stable toward abstraction on NH^+ and NH_2^+ by 0.96 eV and 0.18 eV, respectively, whereas the proton affinity of the trication is substantially higher, 1.98 eV. The mass spectra of aniline were recorded with 1300 nm, 20 fs pulses over the peak intensity range of 1×10^{13} W cm^{-2} to 3×10^{14} W cm^{-2}. The analysis of the mass spectra suggests high stability of both dication and trication to fragmentation. The formation of the fragment NH^+ and NH_2^+ ions is found to proceed via Coulomb explosion.

1. INTRODUCTION

Aniline is widely used for production of synthetic dyes, rubber processing chemicals, herbicides, and methylene diphenyl diisocyanate, a chemical used in the production of polyurethanes for many applications.[1,2] Aniline is also a simple model for the ultraviolet (UV) absorbing chromophore of DNA nucleobases.[3,4] Therefore, the electronic ground and excited states of aniline have been the subject of numerous theoretical[5-14] and experimental[15-18] studies. For instance, recent investigations of the UV photochemistry of aniline have determined that N—H bond fission proceeds through ultrafast, sub-picosecond relaxation from the $\pi\sigma^*$ (S_2) state.[19-22]

Although a large amount of work has been devoted to experimental measurements of the ionization energy of aniline [23] and dissociation products of aniline cation,[24-27] the structures and reaction energetics of positively charged aniline ions have received less attention. The structure and vibrational spectra of the singly charged aniline cation ($C_6H_5NH_2^+$) have been studied at both *ab initio* and density functional theory (DFT) levels,[28] and the energetics of its dissociation into the cyclopentadiene cation ($C_5H_6^+$) and hydrogen isocyanide (HCN) have been studied at the DFT level.[29] Photodissociation spectra of aniline cation have been recorded in the near-infrared (1.30-1.67 eV)[30] and visible (2.73-3.10 eV)[31] regions, with visible excitation forming exclusively $C_5H_6^+$. Both aniline dication and trication were observed in a recent mass spectrometry study using intense 800 nm femtosecond laser pulses for ionization.[32] However, neither the structures nor dissociation pathways of the dication and trication have yet been reported.

In this work, we present the results of a detailed study of aniline and its positively charged ions using DFT calculations and mass spectrometry with intense femtosecond laser excitation. Special attention was paid to the aniline trication because intact molecular trications in mass spectra of small organic molecules containing only one aromatic ring are only rarely observed.[32-35] Theoretical calculations began with a search of the lowest energy isomers of the neutral, singly, doubly, and triply positively charged aniline. We then considered the decay pathways of $C_6H_5NH_2$ and $C_6H_5NH_2^+$ into NH and NH_2, and the decay pathways of $C_6H_5NH_2^{2+}$ and $C_6H_5NH_2^{3+}$ into NH^+ and NH_2^+. It was found that the decay processes

yielding NH and NH^+ proceed through local minima and transition states, whereas the abstraction of NH_2 and NH_2^+ may proceed via stretching the C–N bond until it breaks. The abstraction of hydrogen atoms inequivalent by symmetry was considered for two low-energy structures of the trication. In all cases, the corresponding potential energy curves were found to possess the shapes similar to that obtained for the removal of NH_2^+ from the trication. The chemical bonding and charge distributions in the aniline species was analyzed using the Natural Bond analysis. Experimental measurements using 20 fs, 1300 nm laser pulses for ionization obtained saturation of aniline dication and trication yields, consistent with their predicted stability based on our computations. The fragments NH^+ and NH_2^+ were only observed at high laser intensities and were found to form via Coulomb explosion.

2. METHODS

2.1 Experiment

Mass spectra of aniline were measured using 20 fs, 1300 nm laser pulses. This wavelength was chosen because laser excitation at near-infrared wavelengths (1150—1600 nm) has been widely observed to enhance formation of intact singly-charged and multiply-charged molecular cations as compared to excitation at 800 nm.[36-40] The experimental setup has been described in detail in our previous work.[41] Briefly, a commercial Ti:sapphire regenerative amplifier (Astrella, Coherent, Inc.) produced 30 fs, 800 nm pulses. 2.2 mJ of the amplifier output was used to pump an optical parametric amplifier (OPA, TOPAS Prime) to produce 1300 nm, 20 fs, 125 μJ pulses. Energy attenuation to energies as low as 4 μJ was accomplished using a variable neutral density filter. The resulting beam was expanded to a diameter of 22 mm and focused into the extraction region of a linear time-of-flight (TOF) mass spectrometer with a f = 20 cm fused silica lens. The linear polarization of the laser electric field was rotated from being parallel to orthogonal to the ion TOF axis using an achromatic half-wave plate. A 0.5 mm slit in the extraction plate restricted ion sampling to the region of highest intensity. The peak laser intensity at each pulse energy was calibrated by measuring the ion intensities of Xe^{n+} according to a previously reported procedure,[42] achieving intensities in the range of 1.3×10^{13} to 3.0×10^{14} W cm^{-2}. Samples of aniline (≥ 99.5%, Sigma-

Aldrich) were used without further purification and introduced directly into the vacuum chamber (base pressure 2.0×10^{-9} torr) through an effusive source. Due to the low vapor pressure of aniline, the sample holder was heated with resistive heating tape to produce a pressure of 2.0×10^{-7} Torr measured at the microchannel plate (MCP) detector. Mass spectra were recorded with a 1 GHz digital oscilloscope at a sampling rate of 20 giga samples per second (GS/s) (LeCroy WaveRunner 610Zi). Reported mass spectra and ion yields were sampled over 2×10^5 and 2×10^4 laser shots, respectively.

2.2 Computational Details

Our computations were performed using the density functional theory with the generalized gradient approximation (DFT-GGA) as implemented in the GAUSSIAN 09 program.[43] We chose the BPW91 exchange-correlation functional composed of the Becke exchange[44] and the Perdew-Wang correlation[45] because this is a relatively fast DFT method and provides reliable results. In particular, computations of binding energies using standard reference sets have shown[46] that the BPW91 accuracy to be comparable to that of more recently developed exchange-correlation functionals.

In order to verify the reliability of our choice we performed computations of adiabatic ionization energies (AIE) of neutral aniline using the computational methods from three groups: DFT (BPW91), hybrid DFT (B3LYP[47] and CAM-B3LYP[48]), and post-HF (CCSD(T)[49]) and a quite large 6-311++*G(3df)* basis set. The corresponding values 7.47 eV, 7.54 eV, 7.58 eV, and 7.63 eV which have to be compared to the experimental ionization energy of 7.720±0.002 eV.[23] The difference of 0.16 eV between the CCSD(T) and BPW91 values is quite small and it further decreases when going to the differences between the CAM-B3LYP and BPW91 values and finally between the B3LYP and BPW91 values. The latter is only 0.07 eV and one expects that the BPW91 and B3LYP will show a similar accuracy as obtained in our B3LYP calculations for the nitrotoluene isomers and their cations which were found to be in very good agreement with experiment.[50,51] Since the results of BPW91 calculations are less sensitive to the basis set, we chose a smaller 6-311+G*/(12*s*6*p*1*d*/5*s*4*p*1*d*) basis set of triple-ζ quality for most of farther computations. The AIE with this basis is 7.445 eV; that is, the difference with the value obtained with the

extended basis is less than 0.03 eV. The computations of were also performed using a somewhat larger balanced split-valence Def2-TZVPP [(11*s*6*p*2*d*1*f*)/5*s*3*p*2*d*1*f*] basis.[52] The AIE value obtained at the BPW91/Def2-TZVPP level is 7.437 eV and practically matches the BPW91/6-311+G* value.

In our computations, each unconstrained geometry optimization was followed by the calculations of the harmonic vibrational frequencies in order to confirm the stationary character of an optimized state. The convergence threshold for total energy was set to 10^{-8} eV and the force threshold was set to the default value of 10^{-3} eV/Å. Transition states were found by either using trial geometries and the optimization option "TS" and/or relaxed potential energy scans. After a transition state was found, it was used as the initial state for the Intrinsic Reaction Coordinate (IRC) computations in order to confirm that the TS is connected to the initial state. If this was not so, a new search for another transition state was performed and so on until the IRC results indicated that the TS found is produced from the initial state. Next, the second state at which the IRC run arrived was used for constructing a trial geometry for a new TS and so on until the dissociation limit was reached. In this way, one obtains continuous pathways from the initial states of the neutral and charged aniline to the final decay products. Local excess spin densities, charges on atoms and bonding patterns were obtained using the NBO suite,[53] which is based on the use of natural atomic orbitals (NAO).

3. RESULTS

3.1. Isomers of Neutral and Charged Aniline

Since neither the structure of aniline dication nor trication has been reported, we performed an extensive search for the lowest energy states of these cations and low-lying isomers. For comparison purposes, we have optimized the similar isomers of the neutral and singly charged aniline. Whereas $C_6H_5NH_2$ and $C_6H_5NH_2^+$ possess the same ground-state geometrical topologies in agreement with previous results,[28,29] the ground states of both $C_6H_5NH_2^{2+}$ and $C_6H_5NH_2^{3+}$ have different geometries with respect to each other and to that of the neutral-cation pair. In the dication, the nitrogen atom prefers the *meta*-substitution of a carbon atom in the benzene ring, i.e., a 3-methylenehydropyridine structure (Fig. 1,

structure highlighted in green). The closest in total energy state of the dication has a seven-membered ring structure of azepine and is higher than the ground state by 0.13 eV. The state with the geometrical structure of the neutral ground-state aniline is higher in total energy by 0.68 eV. In the ground-state trication, the nitrogen atom occupies the *para*-position (4-methylenehydropyridine, highlighted in blue in Fig. 1) and the state with the *meta*-substitution is higher by 0.08 eV. The states with the geometries similar to that of the ground-state neutral and azepine (not shown in Fig. 1) are higher by 0.27 eV and 0.76 eV, respectively. Interestingly, the state with the broken carbon ring structure is higher in total energy by only 0.40 eV. It is also worth noting that both the order of states with similar geometrical structures and the relative energy shifts between isomer states are different in the neutral and cation series.

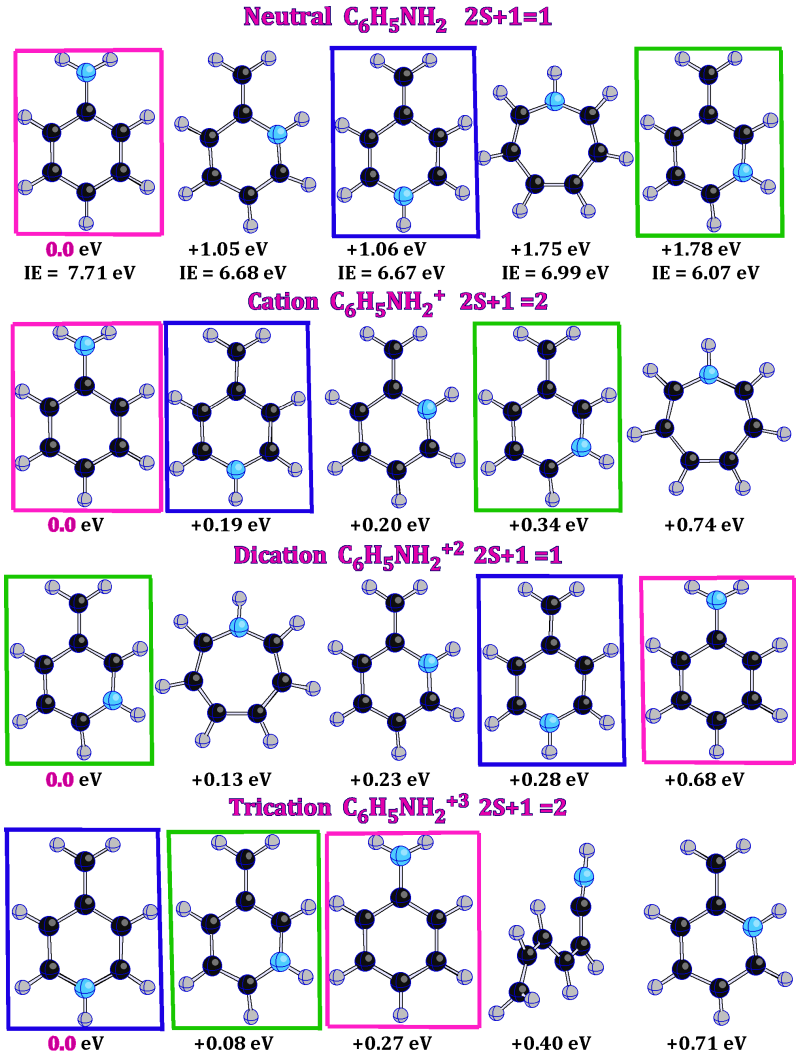

Figure 1. Geometrical structures of the lowest energy isomers of neutral aniline $C_6H_5NH_2$ along with those of its cation $C_6H_5NH_2^+$, dication $C_6H_5NH_2^{2+}$, and trication $C_6H_5NH_2^{3+}$. Total energy shifts (in eV)

are relative to the ground-state total energy of the corresponding series. Ionization energies of the neutral isomer states are in eV. Selected structures are highlighted in boxes: neutral aniline (pink), 3-methylenehydropyridine (green), and 4-methylenehydropyridine (blue).

We have also optimized triplet states for the neutral aniline and its dication along with quartet states for the cation and trication for all isomers shown in Fig. 1. The singlet-triplet splitting of the ground-state neutral and dication computed at the BPW91/6-311+G* level are 3.23 eV and 2.17 eV. The doublet-quartet splitting of the ground-state cation and trication obtained at this level are 3.47 eV and 3.32 eV, respectively. The rest of the splitting values are presented in the Supporting Information, Table S1.

3.2. Dissociation Pathways to NH and NH^+

In order to determine how dissociation of NH depends on the charge of aniline, we compare the pathways leading to the abstraction of NH from the neutral and cation and NH^+ from the dication and trication. For the abstraction of NH from neutral aniline, we found two pathways presented in Fig. 2. The first transition states, labelled **TS1**, are quite similar in both pathways and lead to the same local minimum state **LM1.** There are two subsequent transition states (**TS2** in both pathways) with **LM1** as a predecessor corresponding to different processes of benzene ring rupture. These transition states lead to geometrically different predissociative states (**LM2** in both pathways), which are followed by the transition states (**TS3** in both pathways) corresponding to the aniline dissociation to C_6H_6 and NH but with different isomers of benzene.[54] As can be seen in Fig. 2, the lowest energy activation barrier of 6.65 eV corresponds to pathway **I**, which is above the dissociation limit by 2.82 eV.

Dissociation of the aniline cation and dication to $C_6H_6^+ + NH$ and to $C_6H_6^+ + NH^+$, respectively, proceed in a pathway analogous to that of neutral aniline via pathway **II** when the dication state has the same geometrical topology as the cation and neutral. The only significant difference is the absence of a transition state corresponding to the transition state **TS2** in pathway **II** (see Fig. 3). The activation barrier of the cation is larger than that in the neutral by 0.26 eV, whereas the activation energy of 7.03 eV required for inducing dissociation of the dication to NH^+ is higher by 0.38 eV when compared to the NH

dissociation from the cation and by 0.54 eV from the neutral (*cf.* Figs. 2 and 3). The dissociation pathway for the lowest energy dication isomer can be initiated via its isomerization to the dication isomer with the neutral aniline geometry as shown in Fig. 4 and subsequently proceed according to the pathway in Fig. 3. The dication isomerization proceeds via a seven-membered ring (see Fig. 4) and the transition state **TS2** corresponds to the energy barrier of 5.85 eV. Therefore, one can expect that the aniline dications formed by ionization of the neutral and singly positively charged aniline will retain the geometrical topologies of their precursors.

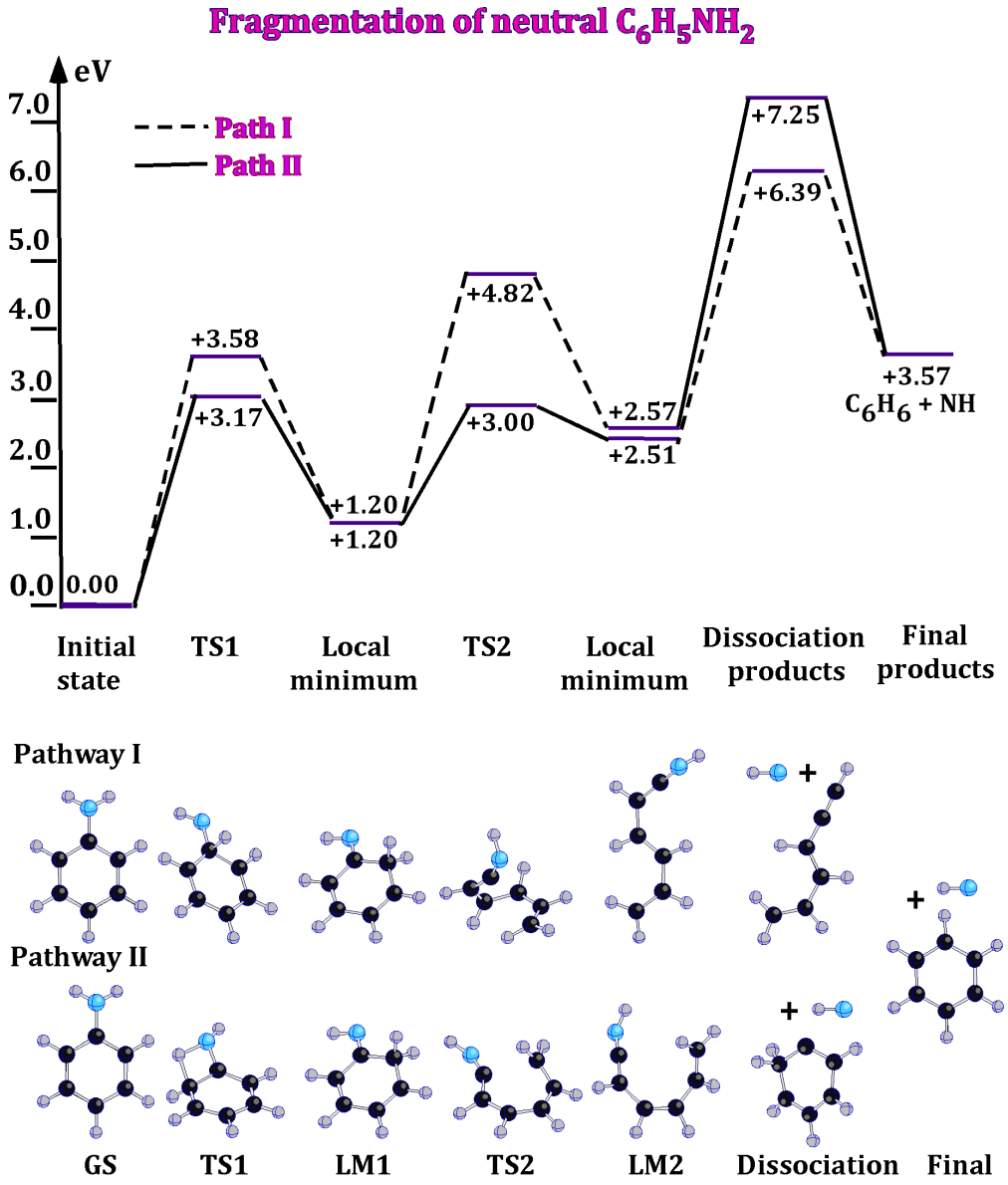

Fig. 2. Two pathways of aniline fragmentation to benzene and nitrogen monohydride. The energies (in eV) of the transition (**TS**) states, intermediate (local minima) states, and dissociation products are given

relative to the ground-state total energy. Geometrical structures corresponding to each pathway are also shown.

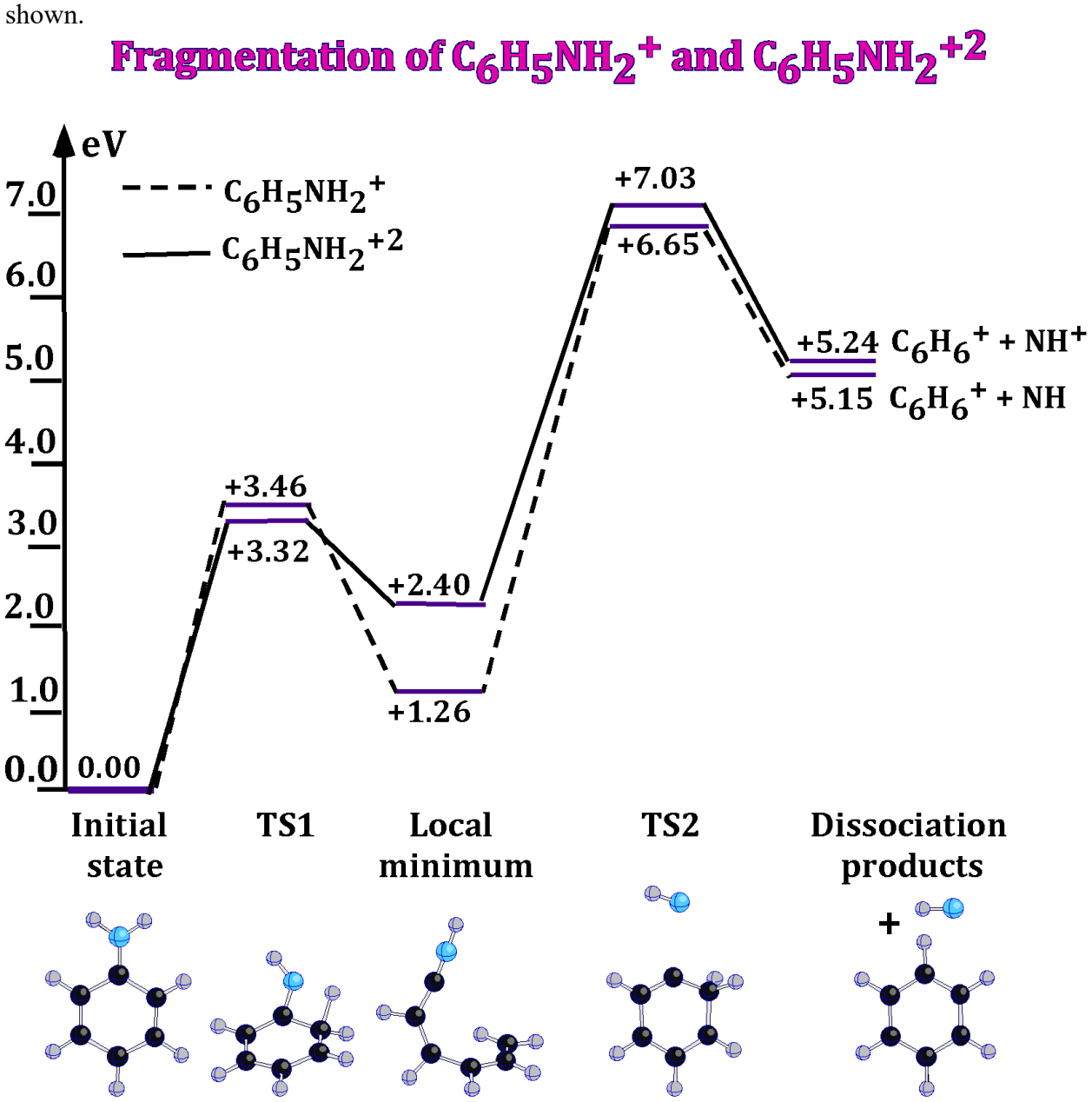

Fig. 3. Pathways of aniline cation and dication decay to $C_6H_6^+$+ NH and to $C_6H_6^+$ + NH^+, respectively. The energies of the transition (TS) states, the intermediate local minimum states, and the dissociation products are given with respect to the total energy of the cation ground state in the case of the cation pathway. In the case of the dication, these energies are given with respect to the total energy of the dication isomer state with the same topology as that of the cation. The geometrical structures corresponding to both pathways are similar.

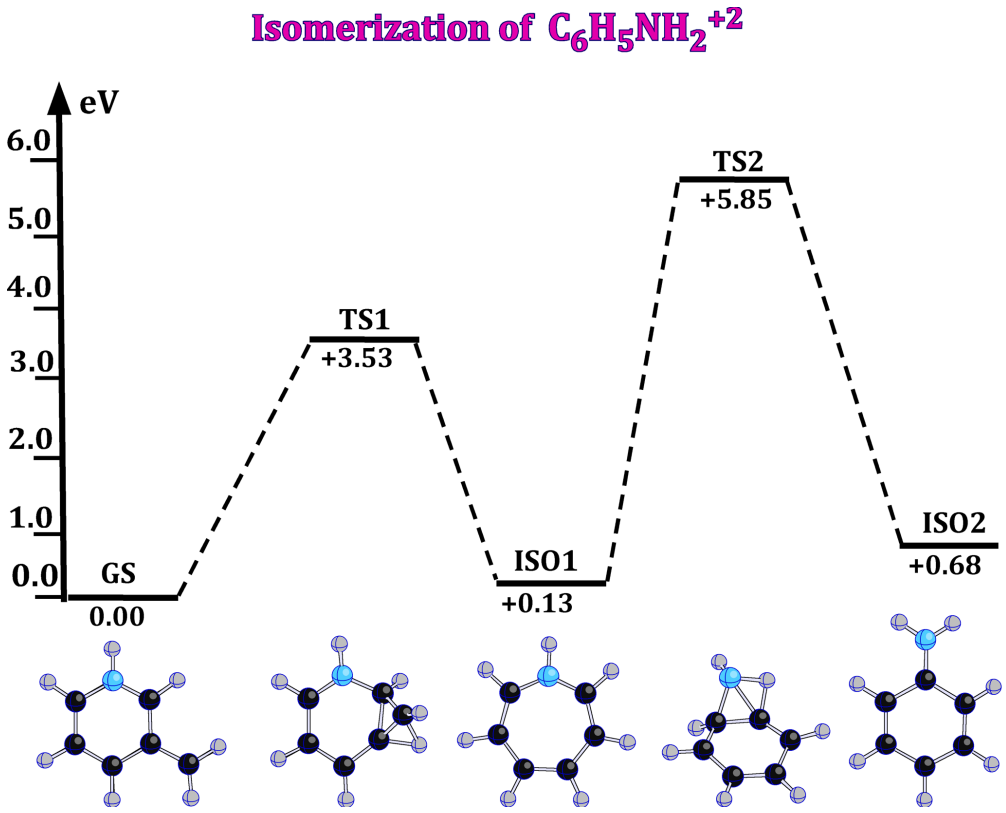

Fig. 4. Isomerization of the aniline dication beginning with its ground state and ending up with the isomer possessing the neutral aniline topology. The energies (in eV) of the transition (**TS**) and isomer (**ISO**) states are given relative to the total energy of the ground-state dication.

The abstraction of NH^+ from the ground-state trication and the isomer of $C_6H_5NH_2^{3+}$ with the geometrical topology of neutral aniline (which is 0.27 eV higher in energy) proceeds via the two transition states shown in Fig. 5. The dissociation barrier height is somewhat lower when the initial geometry is that of the neutral aniline. As can be seen, the final products are presented by two isomers of $C_6H_6^{2+}$, neither of which corresponds to the lowest energy isomer of the dication, which has the shape of a pentagonal pyramid.[55,56] Two pathways leading from these two isomers of $C_6H_6^{2+}$ to the ground-state isomer are shown in Fig. 6. The transition from the isomer in which the carbon atom with two attached hydrogens is in the ortho-position with respect to the hydrogen-free carbon atom to the ground state isomer proceeds via an intermediate state with the benzene hexagonal ring (the top panel in Fig. 6). On the contrary, the intermediate local minimum state in the second pathway possess the geometry of a strongly distorted benzene ring and requires crossing a barrier higher by 0.61 eV (1.26 eV vs 1.91 eV).

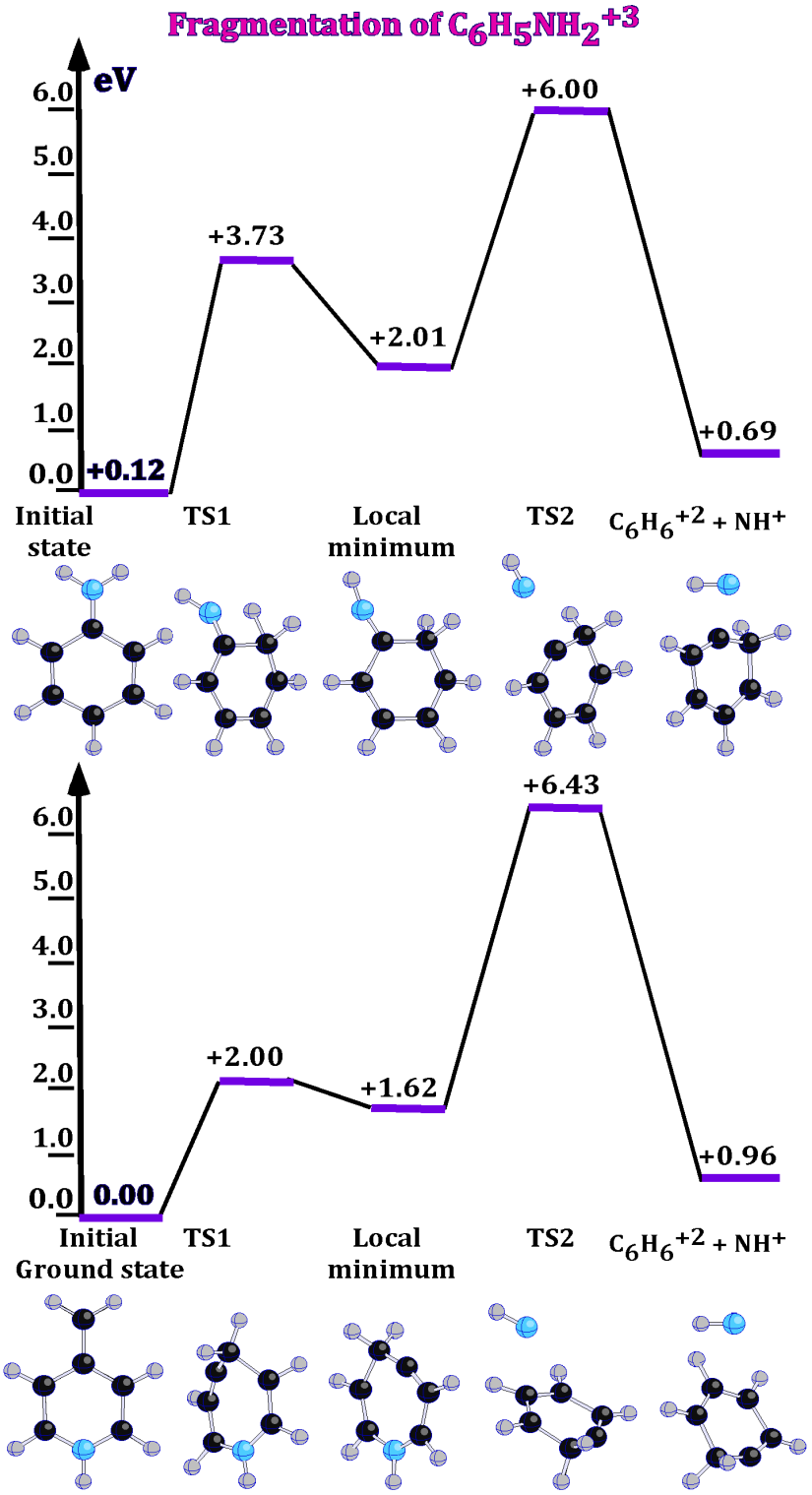

Fig. 5. Pathways of the decay of two lowest energy isomers of the trication to $C_6H_6^{2+} + NH^+$. The energies of the transition (TS) states, the intermediate local minimum states, and the dissociation products are given with respect to the total energy of the corresponding initial isomer states.

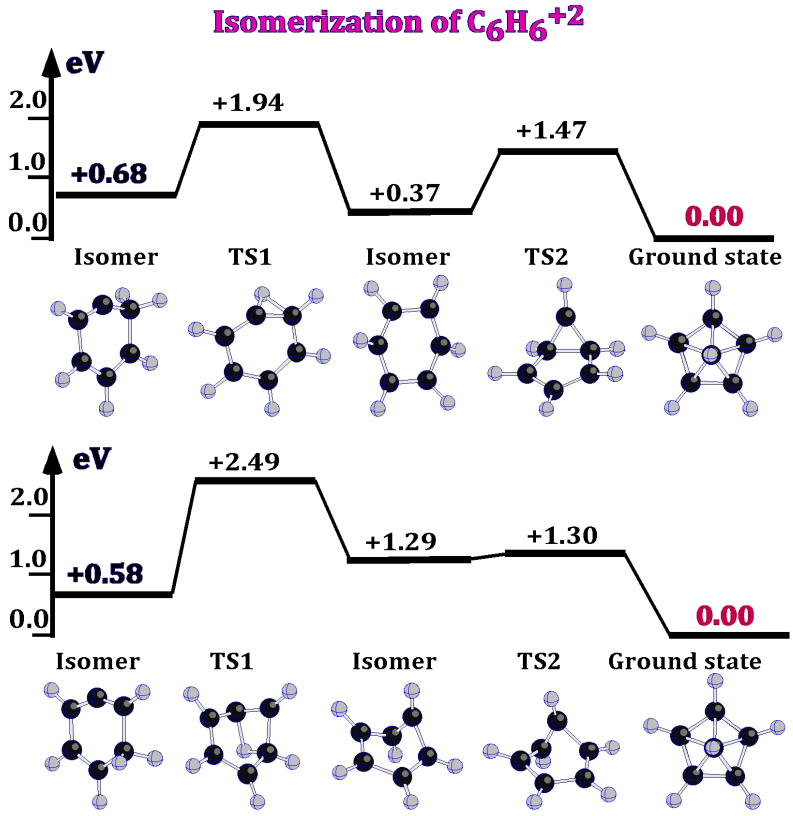

Fig. 6. Isomerization of the benzene dication beginning with the isomers forming in the process of the trication decay (see the preceding figure). The energies (in eV) of the transition (**TS**) and isomer states are given relative to the total energy of the ground-state of $C_6H_6^{2+}$.

Summarizing the data presented in Figs. 2, 3 and 5, the decay energies for the channels C_6H_6–NH, $C_6H_6^+$–NH, $C_6H_6^+$–NH^+, and $C_6H_6^{2+}$–NH^+ are 3.57 eV, 5.15 eV, 5.24 eV, and 0.96 eV, respectively. The latter values were computed in the standard way with accounting for the zero-point vibrational energies obtained within the harmonic approximation, i.e., as

$$D_0(A–B) = E^{el}_{tot}(A) + E_0(A) – [E^{el}_{tot}(B) + E_0(B)] \quad (1)$$

where E^{el}_{tot} is the total Born-Oppenheimer energy and E_0 is the zero-point vibrational energy. The barriers to dissociation, however, are significantly higher than these decay energies for all charge states.

3.3. Abstraction of NH_2 and NH_2^+

In order to gain insight into dissociation of aniline to $C_6H_6 + NH_2$, aniline cation to $C_6H_6^+ + NH_2$, aniline dication to $C_6H_6^+ + NH_2^+$, and aniline trication to $C_6H_6^{2+} + NH_2^+$, respectively, we used a relaxed potential energy scan procedure where the distance between the carbon atom of the ring to which the

amine group is attached and the nitrogen atom is increased from 0.9 Å to 7.0 Å with a step of 0.1 Å. All geometrical parameters were optimized at each step except for the C – N distance. In all cases, the initial structure corresponded to the ground-state geometry of aniline, i.e., $C_6H_5 – NH_2$, of C_{2v} symmetry.

For each species we obtained potential energy curves of the ground states (singlet or doublet, depending on the charge), presented in Fig. 7. The potential energy curves have the shapes typical for diatomics in the case of the neutral and singly charged cation, whereas the dication and especially trication curves do not approach to the asymptotic limit at R(C – N) = 7.0 Å. Dissociation limits computed with eq 1 are 4.29 eV, 4.93 eV, 4.11 eV and 0.18 eV for the neutral, cation, dication, and trication, respectively. Note that the trication curve slowly decreases in energy as the R(C – N) distance increases, and the highest value of 4.7 eV, which can be related with the reaction barrier, corresponds to R(C – N) = 2.9 Å. Since there is no additional activation energy barrier, the NH_2 dissociation from aniline and its cation as well as NH_2^+ from the dication and trication is due to stretching the C – N bond. On the contrary, dissociation to NH and NH^+ proceeds via several transition states, all of which require activation energies that are higher than those required for the NH_2 and NH_2^+ dissociation (see Figs. 3 and 5). It is noteworthy that the energy barriers required for both NH and NH_2 dissociation from the aniline cation are higher than the computed barrier for $C_5H_6^+$ + HNC formation of 3.23 eV.[29] This result is consistent with previous mass spectrometry studies indicating higher yields of $C_5H_6^+$ compared to phenyl and benzene cations,[24-27,31,32] as well as with our experimental results (see Section 3.7).

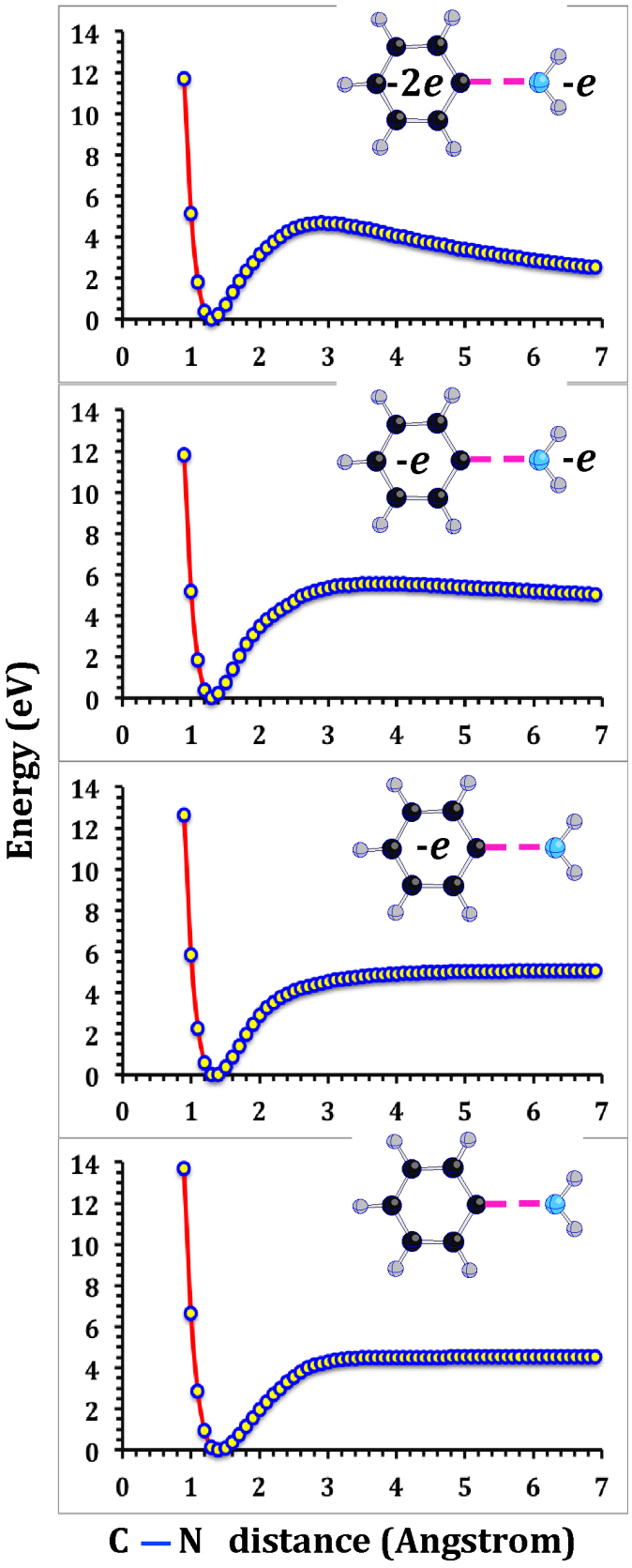

Fig. 7. Potential energy curves corresponding to the C – N bond stretch in ground-state aniline (C_s, $^1A'$) and cation (C_{2v}, $^2B_1$) as well as in the isomers of the dication (C_{2v}, $^1A_1$) and trication (C_s, $^2A''$) with the geometrical topologies of ground-state aniline.

3.4 Stability of the Aniline Trication

In addition to testing the trication stability with respect to the abstraction of the NH_2^+, we also assessed its stability toward abstraction of hydrogens. With this aim, we obtained the C – H and N – H potential energy curves in the ground C_{2v} state of the trication and its isomer with the topology of the neutral aniline, which distorts from C_{2v} to C_s due to an out-of-plane corrugation. There are four H atoms nonequivalent by symmetry in each case. The curves are obtained by a relaxed potential energy scan in which the C– X bond is stretched with a step of 0.1 Å while optimizing the rest of geometrical parameters at each step. As seen in Fig. 8, the potential energy curves obtained in our computations all possess a similar shape. They have a hump at distances around 3.0 Å and energy slowly decreases as the C—X distance further increases. The humps can be identified with the dissociation barriers and they vary from 3.55 eV to 4.80 eV, being higher for the ground-state trication, where the lowest barrier height is 4.3 eV. Since the dissociation process corresponds to the formation of the $C_6NH_6^{2+}$ and H^+ products, then the dissociation limit equals the proton affinity of the trication which can be computed as

$$PA = E_{tot}^{el}(C_6H_5NH_2^{3+}) + E_0(C_6H_5NH_2^{3+}) - [E_{tot}^{el}(C_6NH_6^{2+}) + E_0(C_6NH_6^{2+}) \quad (2)$$

where E_{tot}^{el} is the total Born-Oppenheimer energy, E_0 is the zero-point vibrational energy, and the $C_6NH_6^{2+}$ dication is in its ground state. We performed an intensive search for this ground state and found that the lowest energy state has a C_6H_5 – NH topology of C_{2v} symmetry. The PA value of the ground-state aniline trication computed according eq 2 equals 1.98 eV.

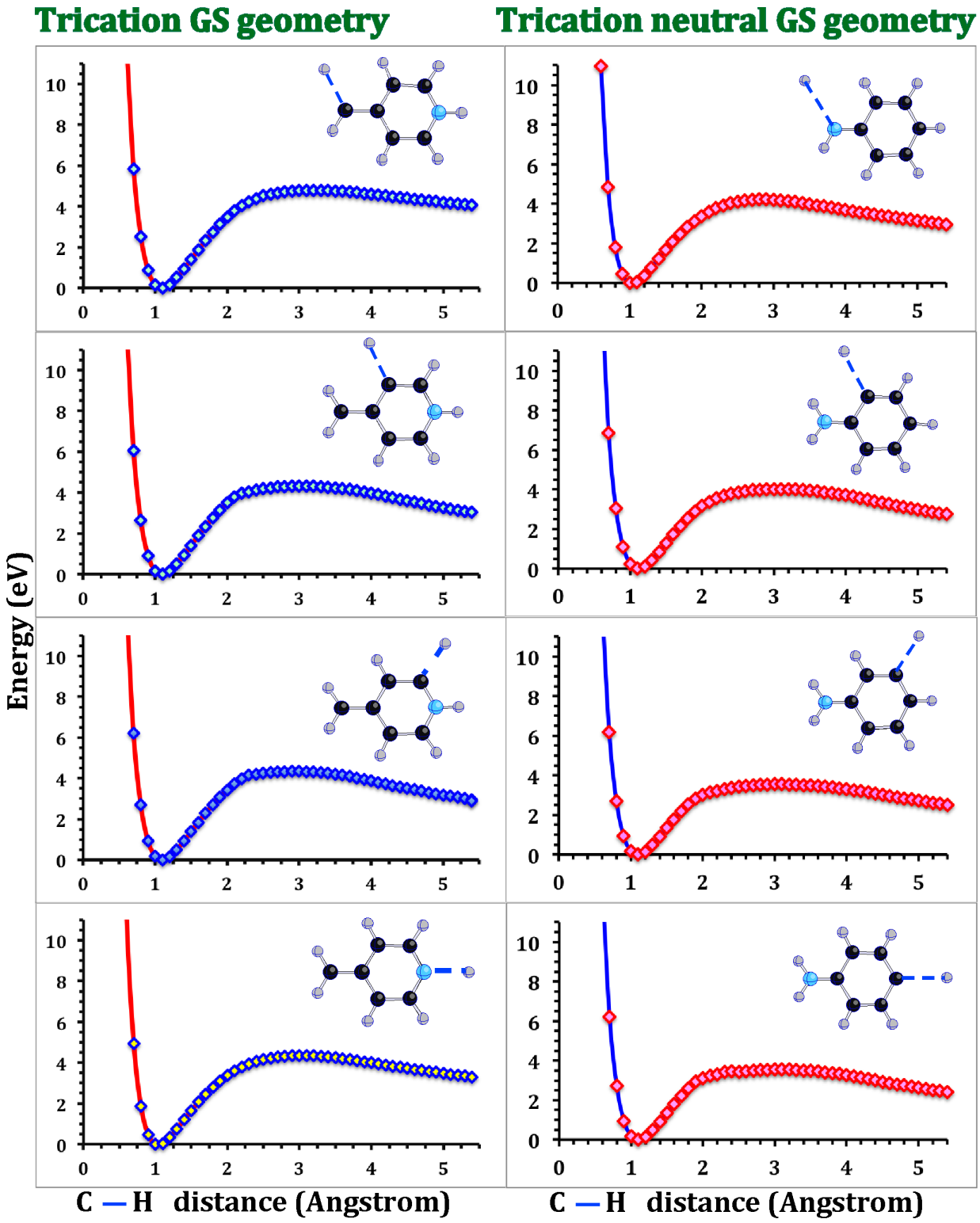

Fig. 8. Potential energy curves corresponding to the C – H bond stretches in the ground-state $C_6H_5NH_2^{3+}$ trication and its isomer with the neutral ground-state topology. The ground and isomer state geometries have C_{2v} and C_s symmetries, respectively. There are four nonequivalent by symmetry H sites in both cases.

Since the geometrical structure of the neutral aniline, which is the initial experimental state, is different from the ground-state geometrical structure of the aniline trication, we performed a search for the lowest energy pathway for the interconversion of these two geometrical structures (Fig. 9). Both pathways contain intermediate local minima states with the azepine geometrical structures as the final step to produce the trication with the neutral aniline geometry, resulting in the same barrier height of 5.15 eV. Therefore, it is expected that the trication in our experiments has the geometry of the neutral.

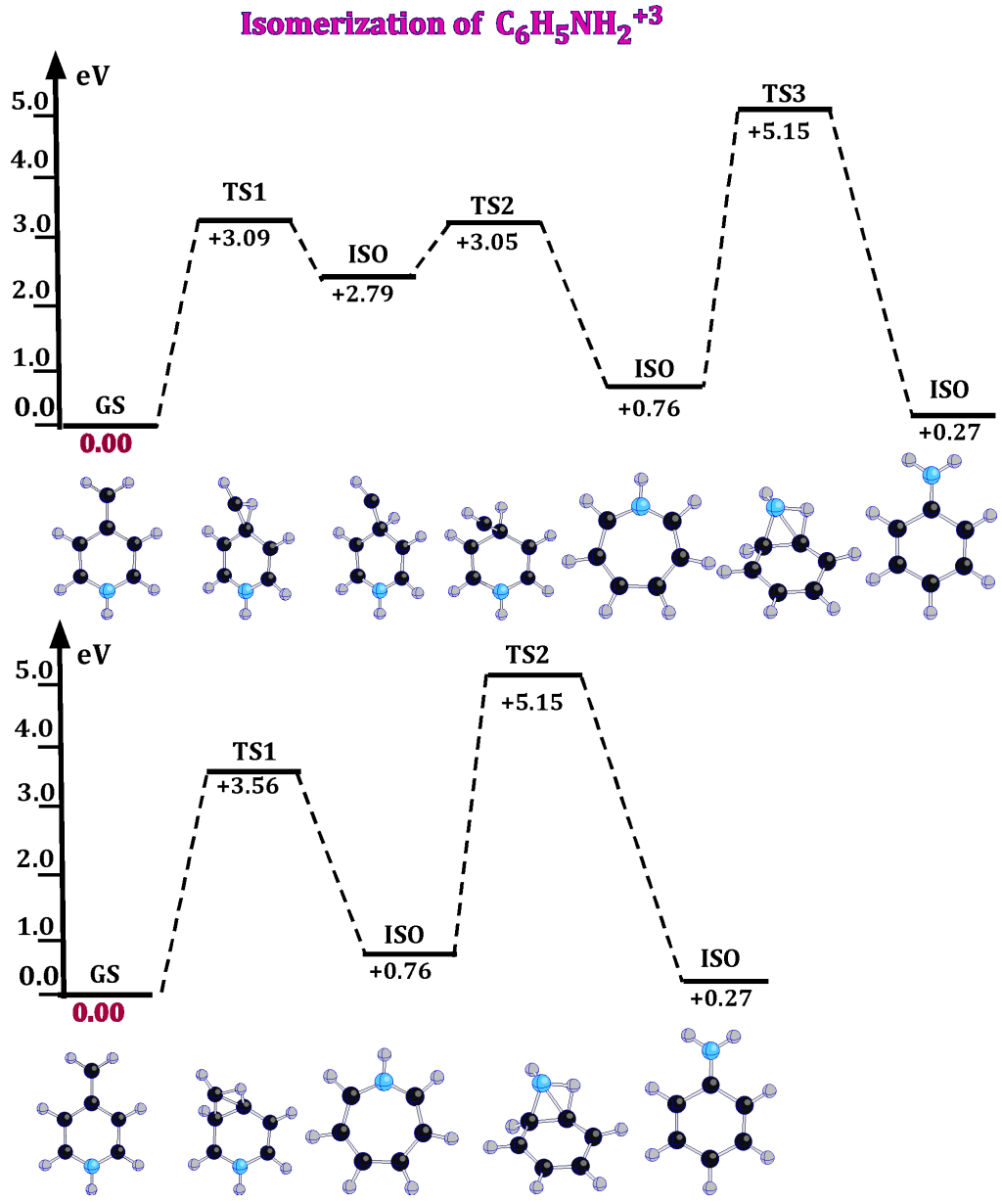

Fig. 9. Two pathways of isomerization of the aniline trication beginning with its ground state and ending up with the isomer with the topology of the neutral aniline ground state. The energies (in eV) of the transition (**TS**) and isomer (**ISO**) states are given relative the total energy of the ground-state trication.

3.5. Electron Affinity and Ionization Energy

When considering one-electron oxidation and reduction of aniline, Raczyńska et al. have postulated the existence of stable singly negatively charged aniline isomers.[57] Using geometrical structures of the isomers from their work, which are higher in total energy than the isomers in Fig. 1, and five isomers of the neutral aniline given in Fig. 1, we attempted optimizations of the singly negatively charged aniline states. In all cases the optimized doublet states had the total energies higher than the total energies of the corresponding neutral states. In such a case, either an anion has a metastable state due to differences in geometries between the neutral and anion,[58,59,60] or its existence is an artifact of the computations related to the absence of diffuse functions in the basis set used. By adding to the basis set of the nitrogen atom two diffuse *s*-functions with exponents of 0.01 and 0.001, we found that the eigenvalues of the highest occupied molecular orbitals (HOMO) of all considered anion states are close to zero, which indicates an unbound character of the extra electron and, therefore, the electron affinity of the neutral aniline is zero.

Adiabatic ionization energy (IE_{ad}) is computed as the difference of total energies of the lowest energy state of a species and the lowest energy state of the cation formed after the detachment of an electron from the species. That is, both states are at their equilibrium ground-state geometries. We computed the adiabatic ionization energies for the neutral, cation and dication as

$$IE_{ad} = E_{tot}^{el}(C_6H_5NH_2^{+n}) + E_0(C_6H_5NH_2^{+n}) - [E_{tot}^{el}(C_6H_5NH^{+(n-1)}) + E_0(C_6H_5NH^{+(n-1)}) \quad (3)$$

where n = 0,1, and 2, E_{tot}^{el} is the total Born-Oppenheimer energy at the optimized geometry of each species and E_0 is the zero-point vibrational energy computed in the harmonic approximation. The vertical detachment energies were computed as the differences in total energy at the ground-state neutral geometry according to the formula:

$$IE_{vert} = E_{tot}^{el}(C_6H_5NH_2^{+n}) - E_{tot}^{el}(C_6H_5NH^{+(n-1)}) \quad (4)$$

The IE_{ad} and IE_{vert} values computed at the BPW91, B3LYP, CAM-B3LYP, CCSD(T) levels of theory with the 6-311++*G*(3*df*) basis set are shown in Table 1. The detailed results are presented in Table S2 of the Supporting Information, where the results of our MP2 calculations are also presented. One can see in Table S2 that the approximate wavefunctions built on the Kohn-Sham orbitals possess smaller spin contaminations than those built on HF orbitals in the MP2 method. As for the CCSD(T) results, we found that the largest T-amplitude of 0.3 belongs to $C_6H_5NH_2^+$. This means that the cation ground state is essentially multiconfigurational. The T-amplitudes of all other states are smaller than the empirical threshold of 0.25.

TABLE 1. Adiabatic and Vertical Ionization Energies of the Aniline Series Computed at Four Levels of Theory with the 6-311++G(3df) Basis Set.[a]

	BPW91		B3LYP		CAM-B3LYP		CCSD(T)	
Species	IE_{ad}	IE_{vert}	IE_{ad}	IE_{vert}	IE_{ad}	IE_{vert}	IE_{ad}	IE_{vert}
$C_6H_5NH_2$	7.47	7.75	7.54	7.86	7.58	7.94	7.63	7.95
$C_6H_5NH_2^+$	12.96	13.76	12.96	13.88	13.01	13.96	12.74	13.71
$C_6H_5NH_2^{2+}$	20.56	21.04	20.54	21.06	20.53	21.09	20.74	20.98
$C_6H_5NH_2^{3+}$	…	27.21		27.13		27.26		26.89

[a] All values are in eV.
[b] The adiabatic ionization energy of neutral aniline evaluated over a large set of experimental data is 7.72 eV, and the experimental vertical ionization energies are in an 8.02-8.10 eV range.

As can be seen in Table 1, all corresponding IE_{ad} and IE_{vert} values computed at the BPW91, B3LYP and CAM-B3LYP levels agree with each other within 0.1 eV whereas the agreement with the corresponding CCSD(T) values are within 0.2-0.3 eV. One can notice that the adiabatic corrections to the IEs of the cation and dication are larger than the adiabatic correction of the neutral aniline. This can be attributed to different topologies of the species (see Fig. 1). It is interesting that the energy intervals between the IE_{vert} are all close to 6.0 eV.

3.6. NBO ANALYSIS

A natural bonding orbital (NBO) analysis for the neutral aniline, its radical cation and the aniline dication with the neutral aniline geometry was performed in order to gain more insight in the changes of the electronic structure of the neutral aniline due to its ionization. In these three cases, the nitrogen atom was attached to the carbon ring as a part of primary amine functional group. In addition, we performed an

NBO analysis of the rearranged dication, which can be described as a 3-methylenehydropyridine (3MP) structure with one methyl hydrogen moved to the nitrogen (Fig. 1, green). In the case of the rearranged trication, the lowest energy state can be described as a 4-methylenehydropyridine (4MP) (Fig. 1, blue). An NBO analysis of the neutral aniline and its radical cation has previously been performed using the results of B3LYP calculations of Hobza et al.[28] Their charges on atoms obtained are quite close to the corresponding charges reported in this work (compare the numbers between Fig. 10 and Fig. 1 in Ref. [28]). We briefly discuss the changes when going from the neutral to the cation and then focus on the dication and trication states.

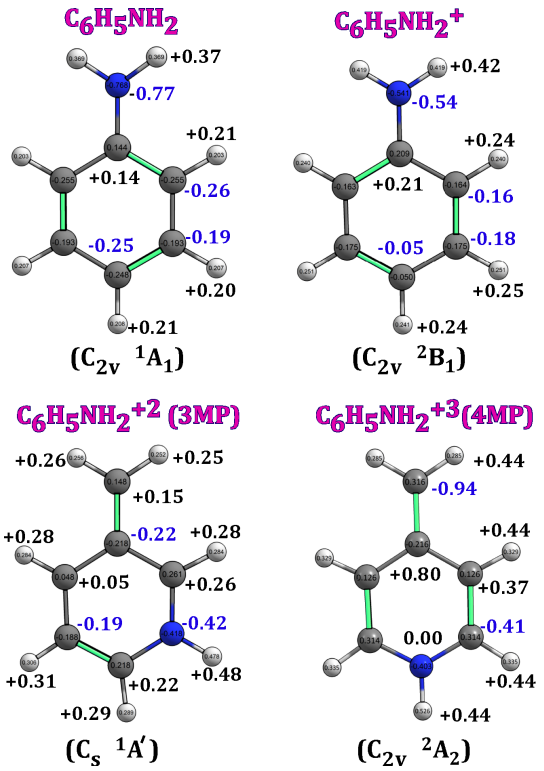

Fig. 10. NBO charges on atoms of aniline, its cation, dication, and trication.

When comparing the NBO charges of atoms between the neutral and radical cation species (Fig. 10), one can notice that the extra positive charge is not localized at any group of atoms. Instead, about a third of the extra charge belongs to the amine group and the other two thirds are delocalized over carbon and hydrogen atoms of the ring. It should be noted that the carbon atoms in the *meta*-position of the neutral aniline are less negatively charged than the carbon atoms in the *ortho* and *para*-positions. This is in line

with what one would expect for a strongly activating group attached to a benzene ring. Both aniline cation and dication seem to be *para*-directing.

In the NBO approach, delocalization effects of the electron density are evaluated using second-order perturbation theory by calculating the off-diagonal Fock matrix elements F_{ij}. The NBO output lists all possible interactions between the occupied Lewis-type bonding orbitals and the nearly empty non-Lewis orbitals. In the case of the neutral aniline, the occupation number of the nitrogen lone-pair (LP_N) is 1.84 and this LP delocalizes partially via an $LP_N \rightarrow LP_{C1}$ electron transfer. The lone pairs on the neighboring carbon (C_1) and the para-carbon (C_4) shown in Fig. 11 are half-filled and their occupancies are 0.98 and 1.05, respectively. The carbon LPs correspond to the highest lying MOs and are nearly degenerate in orbital eigenvalues. The bonding π_{C2C3} orbital within the ring acts as an acceptor for some of the LP_{C1} electron density. In turn, the LP_{C1} has a strong donor-acceptor interaction with the two π^*_{C2C3} antibonding orbitals while the LP_{C4} has a strong $LP_{C4} \rightarrow \pi^*_{C2C3}$ interaction. Within the carbon ring, there are a number of $\pi_i \rightarrow \pi_j^*$ delocalization interactions that are typical of benzene-containing systems.

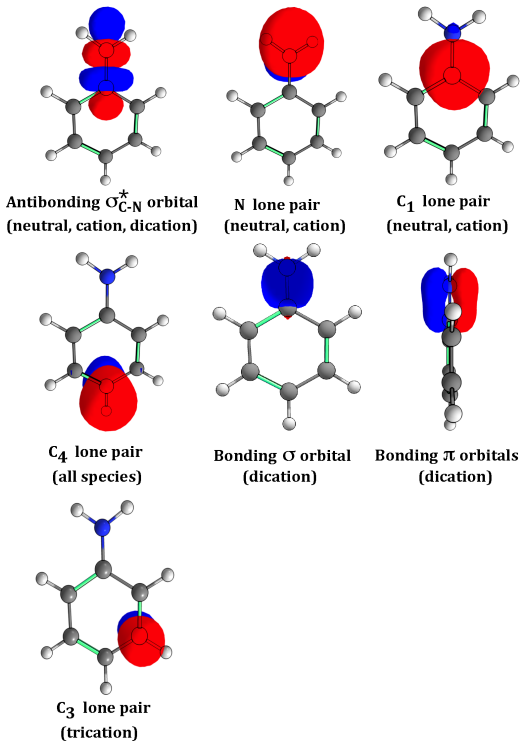

Fig. 11. Important representative bonding, antibonding MOs and lone pairs of aniline $C_6H_5NH_2$, $C_6H_5NH_2^+$ $C_6H_5NH_2^{2+}$, and $C_6H_5NH_2^{3+}$.

Because the ground state of the cationic aniline is a doublet, one has to consider interactions in the α- and β-spin representations separately. When comparing the charges and the orbital compositions obtained from the NBO computations, one can notice that the occupancy of the nitrogen LP decreases to 0.91 and this LP almost entirely belongs to the α-spin representation. As a matter of fact, many of the donor-acceptor interactions in the cation are quite similar to those in the neutral. The major difference is presented by the $LP_N \rightarrow LP_{C1}$ interaction, which becomes stronger by about 15 kcal/mol. The C – N bond shortens by 0.06 Å, which correlates with the loss of 0.0024 *e* by the antibonding σ^*_{CN} orbital and makes the bond stronger. Unlike the neutral case, there are three bonding orbitals of the C($sp^{2.5}$)–N($sp^{1.5}$) type, one in the α-representation and two in the β-representation, that is, the bond order is approximately 1.5 between C and N, all bonds and bond orders are displayed in Figure 12 for clarity. Further NBO analysis is given in the Supporting Information where we provide tabulated results on these bonding interactions (Tables S3-S5) and explain why the 3MP/4MP configurations become more stable in the multiply charged cations.

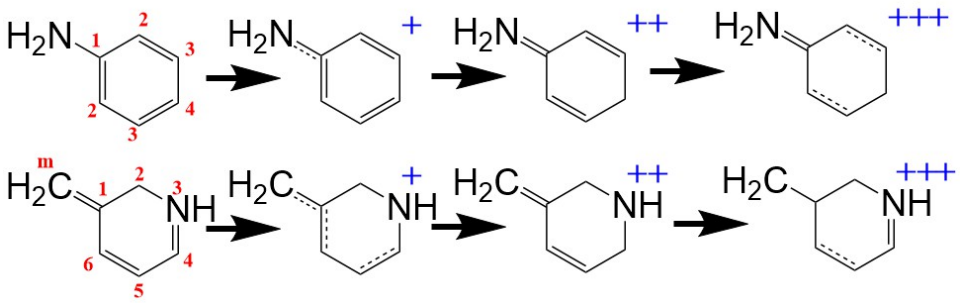

Fig. 12. Row 1: The neutral, cation, dication and trication of aniline. Row 2: neutral, cation, dication and trication of 3MP. Lone pairs were highly delocalized in many cases, as shown in Table S4. The atoms in the first structure are numbered in both rows.

3.7. Experimental Results

Figure 13a shows mass spectra of aniline recorded with 1300 nm, 20 fs pulses at peak intensities of 5×10^{13} W cm^{-2} (50 TW cm^{-2}, dark blue) and 2×10^{14} W cm^{-2} (200 TW cm^{-2}, dark red). The laser polarization was oriented parallel to the TOF axis. The two dominant species at 50 TW cm^{-2} are the aniline parent ion (An^+, *m/z* 93) and dication (An^{2+}, *m/z* 46.5), and magnification shows the presence of the

trication (An^{3+}, *m/z* 31). At 200 TW cm^{-2}, An^{2+} dominates the mass spectrum and An^{3+} is the third most intense peak. Even at this high intensity, fragment ions (other than H^+ and small peaks resulting from contamination by air: H_2O^+, N_2^+, O_2^+, marked with black squares) are barely visible. Magnification of selected *m/z* regions (Figs. 13b-13d) shows these minor fragments indicated at their respective *m/z* values on each plot. All fragments are assigned to singly charged species, with the possible exception of the *m/z* 39 peak, which may consist of a mixture of $C_3H_3^+$ and the benzene dication, $C_6H_6^{2+}$. However, we cannot definitively assign any contribution from the benzene dication in the present measurements, and significant yields of this species are not expected based on the high computed energy barrier to its formation from the aniline trication of 6 eV (see Fig. 5). With the exception of H^+, the fragment ion produced in the highest yield is the cyclopentadiene cation, $C_5H_6^+$, which is in agreement with the previous mass spectrometry studies.[24-27,31,32,61] The significantly lower yields of $C_6H_6^+$ and $C_6H_5^+$ (see Fig. 13d) are consistent with the high computed dissociation barriers (see Figs. 3 and 7) as compared to previous theoretical results on the formation of $C_5H_6^+$.[29]

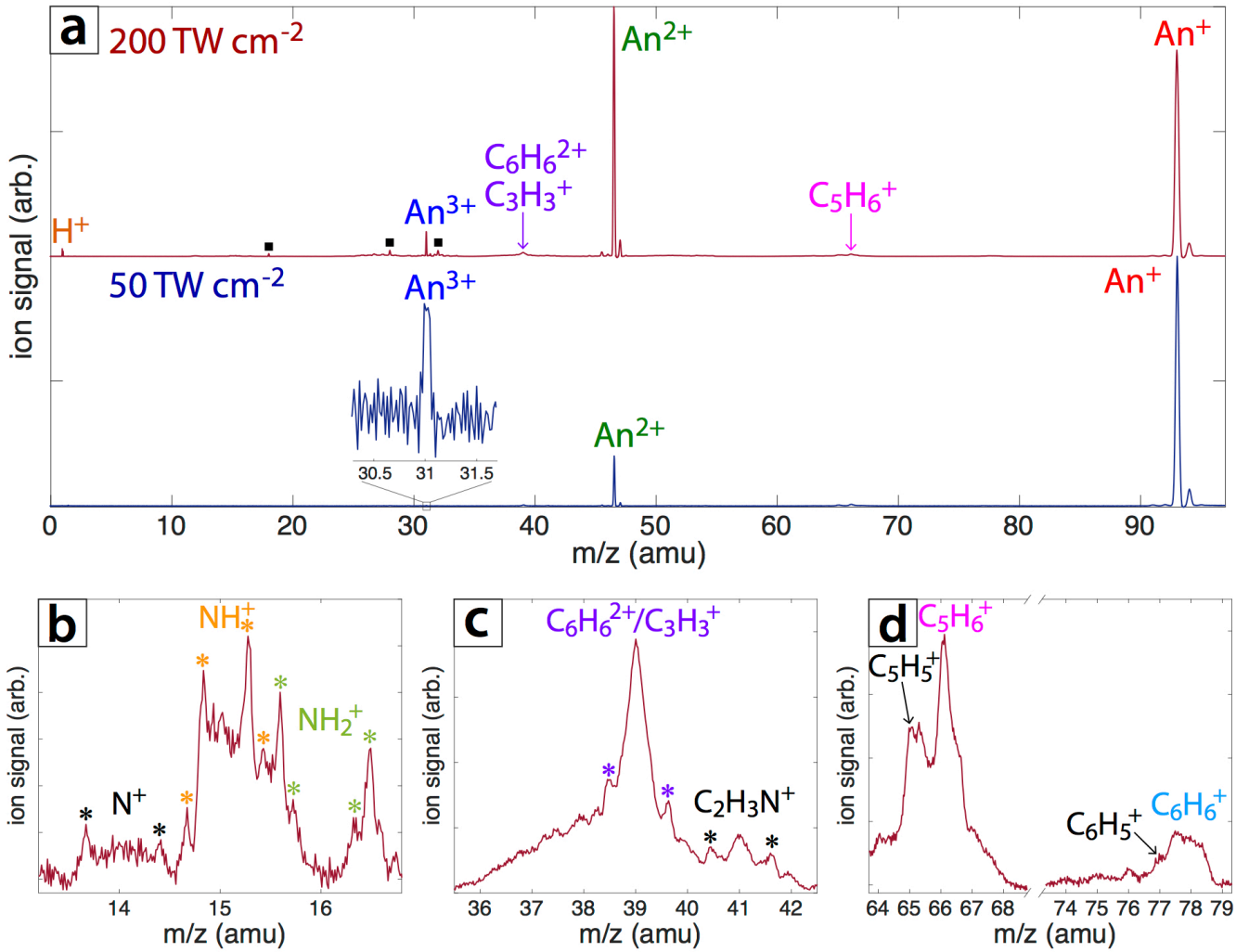

Fig. 13. Mass spectrometry data for aniline: (a) Full mass spectra obtained at intensity 50 TW cm^{-2} (dark blue) and 200 TW cm^{-2} (dark red). (b)—(d) Magnification of selected m/z regions in the 200 TW cm^{-2} spectrum. Coulomb explosion peaks are marked with "*". Peaks attributed to contamination from air are marked with black squares.

Fragments including $C_3H_3^+/C_6H_6^{2+}$ (violet in Fig. 13c), NH_2^+ (green in Fig. 13b), and NH^+ (orange in Fig. 13b) exhibit multiple peaks, indicating their formation from via Coulomb explosion of multiply charged precursors.[62-66] The split peaks marked with a symbol "*" appearing below and above the nominal *m/z* values arise from energetic fragments preferentially ejected towards and away from the detector, respectively, upon precursor breakup. Both NH_2^+ and NH^+ fragments exhibit a two pairs of Coulomb explosion peaks. To further investigate the origin of these peaks, we measured additional mass spectra with the laser polarization orthogonal to the TOF axis. When the precursor ion has a longer lifetime than the rotational periods (89, 193, and 281 ps for aniline), energetic fragments released by Coulomb explosion

are ejected isotropically. In contrast, when fragmentation occurs faster than the timescale of rotation, energetic fragments are ejected preferentially along the laser polarization direction. Therefore, suppression of Coulomb explosion peaks with orthogonal laser polarization indicates fast precursor breakup within a rotational period, whereas Coulomb explosion peaks observed under both polarization conditions indicate slow precursor breakup.[66] Figure 14 shows magnification of the *m/z* 14-17 region of the mass spectra taken at 100 (bottom) and 200 (top) TW cm^{-2} with parallel (red) and orthogonal (blue) laser polarization. At 200 TW cm^{-2}, five pairs of Coulomb explosion peaks, labeled **A** through **E**, are visible. The peaks **A** (N^+), **B** (NH^+), **D** (NH_2^+), and **E** (NH_2^+) are either absent or significantly suppressed under orthogonal polarization as compared to parallel polarization, indicating they arise from fast precursor breakup. In contrast, peaks **C** (NH^+) are still present under orthogonal polarization, even at intensities as low as 100 TW cm^{-2}. This result indicates that there exists a slow (i.e., longer than several hundred ps) dissociation pathway from a multiply charged aniline ion that forms NH^+. The calculated kinetic energy released from each dissociation pathway based on the difference in flight time between the two peaks[36] are given in Table 2, with further details about the methods and estimated error given in the Supporting Information, Table S6. The pairs **A**, **B**, and **D** corresponding to fast processes release significantly more kinetic energy (~9-11 eV) than the slow process from pair **C** that releases only ~3 eV.

TABLE 2. Calculated kinetic energy release (E_k) of Coulomb explosion for peaks identified in Fig. 14

fragment	label	E_k (eV)	timescale[a]
N^+ (*m/z* 14)	A	9.7±0.6	fast
NH^+ (*m/z* 15)	B	8.8±0.6	fast
	C	3.0±0.3	slow
NH_2^+ (*m/z* 16)	D	10.9±0.6	fast
	E	4.8±0.4	fast

[a] denotes timescale relative to rotational period of aniline (~90—300 ps)

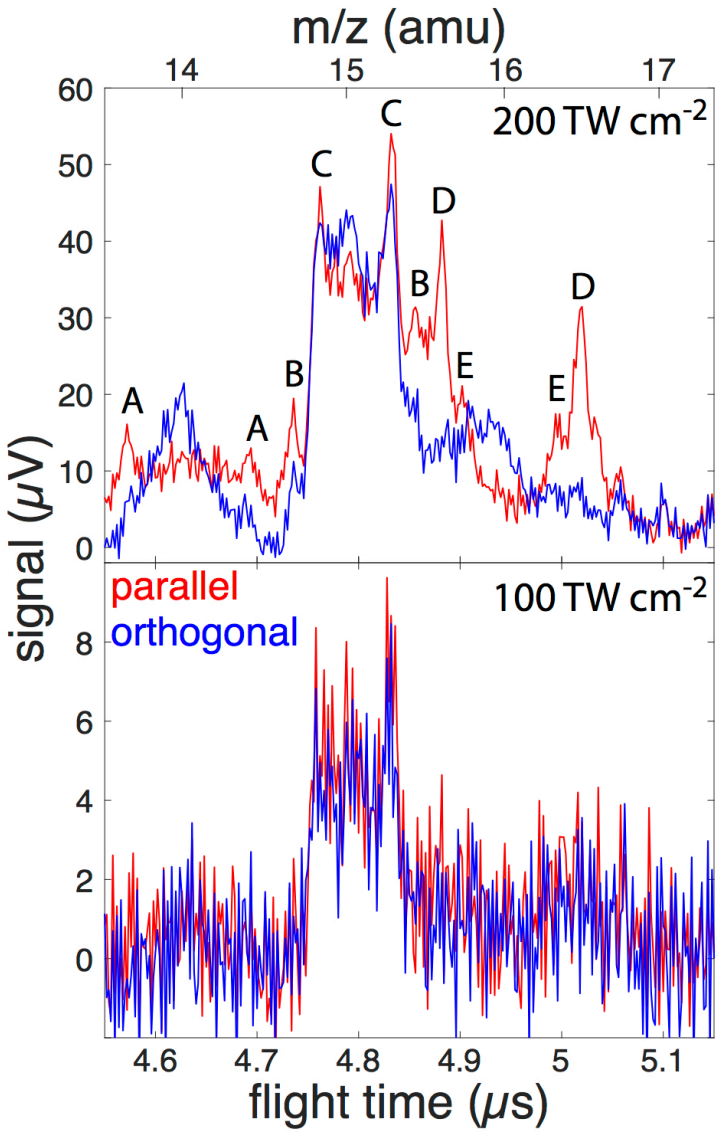

Fig. 14. Magnified mass spectra of the *m/z* 14 – 17 region taken with the laser polarization parallel (red) and orthogonal (blue) to the TOF axis. The labels **A** through **E** denote distinct pairs of Coulomb explosion peaks with computed kinetic energies listed in Table 2.

The integrated ion yields of the three parent ion charge states and major fragments as a function of peak intensity are shown in Fig. 15. All yields are normalized to that of the singly charged parent ion at the highest intensity of ~300 TW cm^{-2}. The yields of all three parent ion charge states saturate at sufficiently high intensities of ~100 TW cm^{-2} for An^+, ~180 TW cm^{-2} for An^{2+}, and ~300 TW cm^{-2} for An^{3+} (Fig. 15, top). The yields of An^{2+} and An^{3+} saturate respectively at ~83% and ~12% of the saturated An^+ yield at 300 TW cm^{-2} according to Fig. 15. To account for the increased detector sensitivity of fast ions that can artificially enhance the relative An^{2+} and An^{3+} yields, we used the method of Krems *et al.*[67]

to compute the relative detection efficiencies of An^+, An^{2+}, and An^{3+} (details given in Supporting Information, Table S7). Including this correction, the relative An^{2+} and An^{3+} yields are ~70% and ~9%, respectively. From Fig. 15, it is evident that the fragment ions $C_5H_6^+$ (*m*/z 65, magenta) and $C_3H_3^+$ (*m*/z 39, violet) appear at ~40 TW cm^{-2}, in between the appearance energies of the dication and trication (denoted by the green and blue dotted lines at ~24 and ~50 TW cm^{-2}, respectively). In contrast, the remaining fragments do not appear until ~70 TW cm^{-2} or higher intensities. At intensities above 200 TW cm^{-2}, the yields of small fragments (NH_2^+, NH^+, and H^+) show no signs of saturation, in contrast to the slowing growth of the $C_5H_6^+$, $C_6H_6^+$, and $C_3H_3^+/C_6H_6^{2+}$ signals.

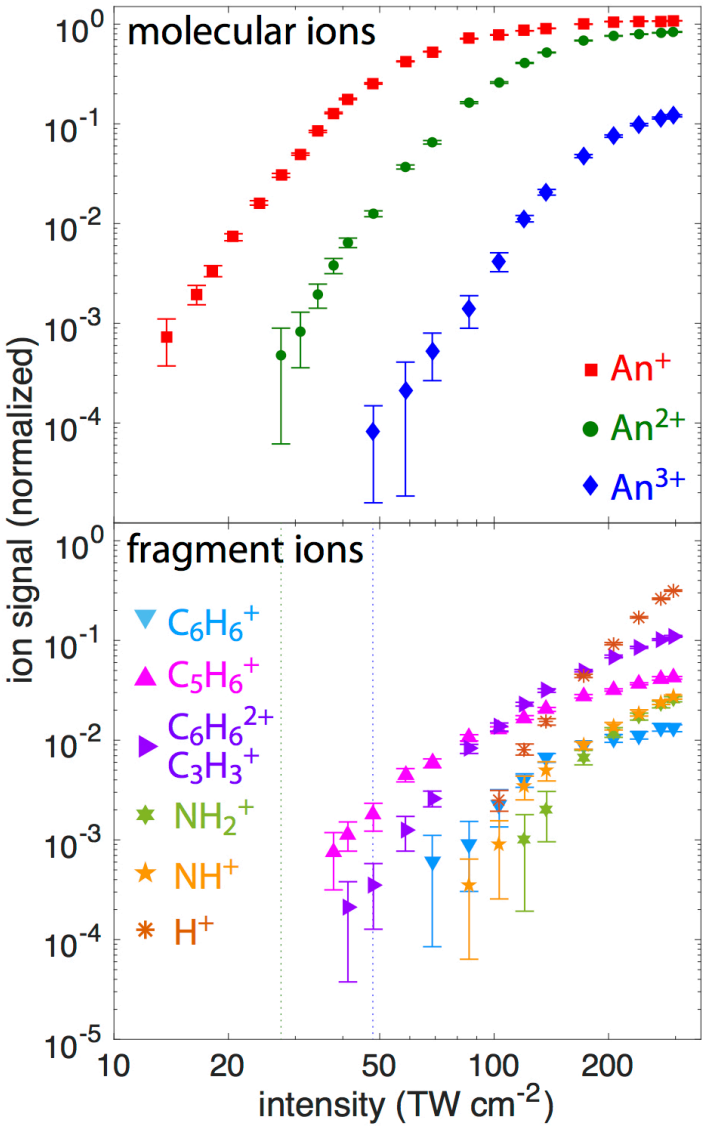

Fig. 15. Integrated ion yield of aniline: (a) aniline cation, dication, and trication; (b) fragment ions. All yields normalized to the aniline cation yield at 200 TW cm^{-2}.

4. DISCUSSION

Our computational results on multiply charged aniline cations can explain the high yields observed in mass spectra both in Fig. 13 and in previous investigations.[32,61] Due to the high interconversion barriers between the neutral C_6H_5–NH_2 geometry and optimal dication and trication geometries of 5.85 eV and 5.15 eV, respectively (Figs. 4 and 6), these multiply charged cations retain the neutral geometry under experimental conditions. At the neutral geometry, both the dication and trication exhibit dissociation barriers of 3 eV or higher to the loss of NH^+, NH_2^+, and H^+ (Figs. 3, 5, 7, 8), making the intact multiply charged cations sufficiently stable to be detected with TOF mass spectrometry. This high stability of aniline up to the trication state makes it an ideal system for future investigations into the chemistry of highly charged organic molecular ions.

The observation that the NH^+ fragment (orange in Fig. 15) appears at a considerably lower intensity (~85 TW cm^{-2}) than the NH_2^+ fragment (light green in Fig. 15, ~120 TW cm^{-2}) motivated computational investigations into the dissociation mechanisms of aniline dication and trication leading to these fragments (Sections 3.2 and 3.3). In particular, the observation of a distinct NH^+ signal with no NH_2^+ signal at 100 TW cm^{-2} (Fig. 14, bottom) would suggest that NH^+ loss is more favorable than NH_2^+ loss. For the aniline dication, the total energy barrier required for NH^+ loss is 7.03 eV (TS2 in Fig. 3), whereas the total energy barrier for NH_2^+ loss is 5.55 eV (Fig. 7). For the trication, the NH^+ barrier is 6.00 eV (TS2 in Fig. 5), whereas the NH_2^+ barrier is 4.65 eV (Fig. 7). The computed barriers ~1.5 eV higher for NH^+ as compared to NH_2^+ abstraction is unexpected given the lower appearance intensity of NH^+ in the experiments. This apparent discrepancy could be due to one or more of the following causes: (1) both the NH^+ and NH_2^+ observed in the experiments originate from a higher initial charge state than aniline trication; (2) the effective barriers to NH^+ loss of 4.63 eV in the dication and 3.99 eV in the trication from the local minima in Figs. 3 and 5, respectively, are lower than for the corresponding NH_2^+ loss channels; and (3) direct loss of NH_2^+ could be accompanied by a H atom loss from the NH_2^+ fragment. However, it is unlikely that the

H atom dissociates following NH_2^+ formation because the dissociation energy for $NH_2^+ \rightarrow NH^+ + H$ is 4.76 eV according to our computations. Therefore, we expect that the observed higher yield of NH^+ is mostly due to some combination of explanations (1) and (2). The predominant slow Coulomb explosion process that forms NH^+ (Fig. 14 and Table 2) could be consistent with the multistep mechanisms in Figs. 3 and 5 that would be expected to result in slow dissociation.

Finally, we note that the data in Figs. 13 and 15 taken with 1300 nm, 20 fs pulses display several differences from previously reported mass spectral data on aniline taken with 800 nm, 50 fs pulses.[32,61] First, we observe significantly higher detector-corrected yields of 70% and 9% for An^{2+} and An^{3+} relative to An^+ at ~300 TW cm^{-2}, compared to the (uncorrected) yields of 20% and 0.2% reported by Scarborough et al. using 800 nm fs pulse excitation.[32] Second, we observe less fragmentation, as evident in comparing the mass spectra in Fig. 13a with those in previous work.[32,61] The suppressed fragmentation and increased yields of intact singly and multiply charged cations observed in our measurements are consistent with previous measurements of polyatomic cations using strong-field excitation in the near-IR region of ~1150-1600 nm as compared to 800 nm.[36-40,63] These results indicate that intense near-infrared excitation can effectively prepare intact highly charged molecular cations that may be subsequently probed with optical excitation to elucidate their dissociation pathways.

5. CONCLUSION

Our systematic study of the structure and properties of neutral, singly, doubly and triply positively charged aniline and their isomers was performed using the all-electron density functional theory with the generalized gradient approximation (DFT-GGA) and a basis set of triple-ζ quality. We first identified a large number of low-energy geometrical structures in the cations and then computed the mechanisms for NH/NH^+ and NH_2/NH_2^+ loss from these structures. The dissociation energies of NH from the neutral and cation are 3.57 eV and 5.15 eV, respectively, while the dissociation energies of NH^+ from the dication and trication are 5.24 eV, and 0.96 eV, respectively. The dissociation energies with respect to the abstraction of NH_2 in the neutral and cation and to NH_2^+ in the dication and trication are 4.29 eV, 4.93 eV, 4.11 eV

and 0.18 eV, respectively. The pathways resulting in the yield of NH and NH^+ contain multiple local minima and transition states, whereas the abstraction of NH_2 and NH_2^+ proceeds via stretching the C–N bond until it breaks. We identified high interconversion barriers for forming the ground-state geometrical structures in $C_6H_5NH_2^{2+}$ and $C_6H_5NH_2^{3+}$ of 5.85 eV and 5.15 eV, respectively, indicating that these cations possess the C_6H_5–NH_2 geometry under experimental conditions. For the trication, barriers to H atom loss were found to be weakly dependent on the position of the H atom in the trication geometrical structure and are around 4.0 eV. That is, the trication has quite a large barrier toward dissociation to H^+, NH^+, and NH_2^+. These high computed dissociation barriers are supported by the photoionization mass spectrometry measurements that obtained saturation of the aniline dication and trication yields at high intensity with negligible associated fragmentation. Collectively, the results from this study indicate that aniline exhibits multiple stable cationic charge states, making it a suitable molecule for studying the dissociation dynamics of highly charged molecular cations.

SUPPORTING INFORMATION

The Supporting Information is available free of charge on the ACS Publications website: Tabulated computed energies for isomers of aniline and its cations; additional discussion and tabulated NBO results; tabulated values for kinetic energy release from Coulomb explosion obtained from mass spectral data; discussion of MCP detector efficiency calculation; geometric coordinates (Z-matrices) for computed aniline structures.

ACKNOWLEDGEMENT

Portions of this research were conducted with high performance computational resources provided by the Louisiana Optical Network Initiative (http://www.loni.org). This research has also used resources of the National Energy Research Scientific Computing Center, a DOE Office of Science User Facility supported by the Office of Science of the U.S. Department of Energy under Contract No. DE-AC02-05CH11231. BRR acknowledges the support from the National Science Foundation under Grant Number OIA-

1541079. KMT acknowledges the support of the U.S. Army Research Office through Contract W911NF-19-1-0099. DAB acknowledges generous financial support from an Altria Graduate Research Fellowship.

AUTHOR INFORMATION

Corresponding Author
*E-mail: kmtibbetts@vcu.edu
*E-mail: gennady.gutsev@famu.edu

ORCID
G. L. Gutsev: 0000-0001-7752-5567
B. R. Ramachandran: 0000-0002-5179-5750
Katharine Moore Tibbetts: 0000-0001-8853-5656
L. G. Gutsev: 0000-0002-9679-9093
Notes
The authors declare no competing financial interest.

REFERENCES

[1] Sénz-Pérez, M.; Lizundia, E.; Laza, J. M.; García-Barrasa, J.; Vilasa, J. L.; Leóna, L. M. Methylene Diphenyl Diisocyanate (MDI) and Toluene Diisocyanate (TDI) Based Polyurethanes: Thermal, Shape-Memory and Mechanical Behavior. *RSC Adv*. **2016,** *6*, 69094-69102.

[2] Maleki, R.; Koukabi, N.; Kolvari, E. Fe_3O_4-Methylene Diphenyl Diisocyanate-Guanidine (Fe_3O_4–4, 4′-MDI-Gn): A Novel Superparamagnetic Powerful Basic and Recyclable Nanocatalyst as an Efficient Heterogeneous Catalyst for the Knoevenagel Condensation and Tandem Knoevenagel-Michael-Cyclocondensation Reactions. *Appl. Organometal Chem.* **2018,** *32*, e3905.

[3] Crespo-Hernández, C. E.; Cohen, B.; Hare, P. M.; Kohler, B. Ultrafast Excited-State Dynamics in Nucleic Acids. *Chem. Rev.* **2004,** *104*, 1977-2020.

[4] Stavros, V. G.; Verlet J. R. R. Gas-Phase Femtosecond Particle Spectroscopy: A Bottom-Up Approach to Nucleotide Dynamics. *Annu. Rev. Phys. Chem.* **2016,** *67*, 211-232.

[5] Niu, E.; Boggs, J. E. The Structure of Aniline. *J. Mol. Struct. (Theochem)*, **1984,** *109*, 381-389.

[6] Wang, Y.; Saebo, S.; Pittman, C. U., Jr. The Structure of Aniline by Ab Initio Studies. *J. Mol. Struct. (Theochem),* **1993,** *281*, 91-98.

[7] Tzeng, W. B.; Narayanan, K.; Shieh, K. C.; Tung, C. C. A Study of the Structures and Vibrations of $C_6H_5NH_2$, C_6H_5NHD, $C_6H_5ND_2$, $C_6D_5NH_2$, C_6D_5NHD, and $C_6D_5ND_2$ in the S_1 State by Ab Initio Calculations. *J. Mol. Struct. (Theochem),* **1998,** *428*, 231-240.

[8] Vaschetto, M. E.; Retamal, B. A.; Monkman, A. P. Density Functional Studies of Aniline and Substituted Anilines. *J. Mol. Struct. (Theochem),* **1999,** *468*, 209–221.

[9] Palafox, M. A.; Gill, M.; Nunez, N. J.; Rastogi, V. K.; Mittal, L.; Sharma, R. Scaling Factors for the Prediction of Vibrational Spectra. II. The Aniline Molecule and Several Derivatives. *Int. J. Quantum Chem.* **2005,** *103*, 394–421.

[10] King, G. A.; Oliver, T. A. A.; Ashfold, M. N. R. Dynamical Insights into $^1\pi\sigma^*$ State Mediated Photodissociation of Aniline. *J. Chem. Phys.* **2010,** *132*, 214307.

[11] Deshmukh, V.; Kharat, B.; Chaudhari, A. Nonlinear Optical Properties and Spectroscopic Characterization of Aniline in Singlet, Triplet and Quintet State using Quantum Chemical Methods. *Comp. Theor. Chem.* **2012,** *980*, 115–122.

[12] Roberts, G. M.; Williams, C. A.; Young, J. D.; Ullrich, S.; Paterson, M. J.; Stavros, V. G. Unraveling Ultrafast Dynamics in Photoexcited Aniline. *J. Am. Chem. Soc.* **2012,** 134, 12578−12589.

[13] Sala, M.; Kirkby, O. M.; Guérin, S.; Fielding, H. H. New Insight into the Potential Energy Landscape and Relaxation Pathways of Photoexcited Aniline from CASSCF and XMCQDPT2 Electronic Structure Calculations. *Phys. Chem. Chem. Phys.* **2014,** *16*, 3122-3133.

[14] Ray, J.; Ramesh, S. G. Conical Intersections Involving the Lowest $^1\pi\sigma^*$ State in Aniline: Role of the NH_2 Group. *Chem. Phys.* **2018,** *515*, 77–87.

[15] Gée, C.; Douin, S.; Crépin, C.; Bréchignac, P. Infrared Spectroscopy of Aniline ($C_6H_5NH_2$) and its Cation in a Cryogenic Argon Matrix. *Chem. Phys. Lett.* **2001,** *338*, 130-136.

[16] Duflot, D.; Flament, J. P.; Giuliani, A.; Heinesch, J.; Grogna, M.; Hubin-Franskin, M. J. C 1*s* and N 1*s* Core Excitation of Aniline: Experiment by Electron Impact and Ab Initio Calculations. *Phys. Rev. A,* **2007,** *75*, 052719.

[17] Rajasekhar, B. N.; Veeraiah, A.; Sunanda, K.; Jagatap, B. N. Excited States of Aniline by Photoabsorption Spectroscopy in the 30 000–90 000 cm^{-1} Region Using Synchrotron Radiation. *J. Chem. Phys.* **2013,** *139*, 064303.

[18] Qu, Z.; Qin, Z.; Zheng, X.; Wang, H.; Yao, G.; Zhang, X.; Cui, Z. Slow-Electron Velocity-Map Imaging Study of Aniline via Resonance-Enhanced Two-Photon Ionization Method. *Spectrochim Acta A. Mol Biomol.* Spectrosc. **2017,** *173*, 432–438.

[19] King, G. A.; Oliver, T. A. A.; Ashfold, M. N. R. Dynamical Insights into $^1\pi\sigma^*$ State Mediated Photodissociation of Aniline, *J. Chem. Phys.* **2010,** *132*, 214307.
[20] Montero, R.; Conde, A. P.; Ovejas, V.; Martínez, R.; Castaño, F.; Longarte, A. Ultrafast Dynamics of Aniline in the 294-234 nm Excitation Range: The Role of the πσ* State. *J. Chem. Phys.* **2011,** *135*, 054308.
[21] Thompson, J. O. F.; Livingstone, R. A.; Townsend, D. Following the Relaxation Dynamics of Photoexcited Aniline in the 273-266 nm Region Using Time-Resolved Photoelectron Imaging. *J. Chem. Phys.* **2013,** *139*, 034316.
[22] Cole-Filipiak, N. C.; Stavros, V. G. New Insights into the Dissociation Dynamics of Methylated Anilines. *Phys. Chem. Chem. Phys.* **2019,** *21*, 14394-14406.
[23] Lias, S. G. NIST Chemistry WebBook, NIST Standard Reference Database Number 69, National Institute of Standards and Technology, Gaithersburg, MD 20899, retrieved May 6, 2019.
[24] Rylander, P. N.; Meyerson, S.; Eliel, E. L.; McCollum, J. D. Organic Ions in the Gas Phase. XII. Aniline. *J. Am. Chem. Soc.* **1963,** *85*, 2723-2725.
[25] Reinhardt, K. L., Jr.; Buchholz, A. C.; Van Lear, G. E. Mass Spectra Fragmentation of Aniline-1-Carbon-13. *J. Am. Chem. Soc.* **1968,** *90*, 1073-1075.
[26] Lifshitz, C.; Gotchiguian, P.; Roller, R. Time-Dependent Mass Spectra and Breakdown Graphs. The Kinetic Shift in Aniline. *Chem. Phys. Lett.* **1983,** *95*, 106-108.
[27] Kühlwind, H.; Neusser, H. J.; Schlag, E. W. Multiphoton Metastable Ion Spectra and Ion Dissociation Kinetics: Analysis of the Decay Channels of Aniline Cation with a Reflectron Time-of-Flight Instrument. *J. Chem. Phys.* **1985,** *82*, 5452-5456.
[28] Wojciechowski, P. M.; Zierkiewicz, W.; Michalska, D.; Hobza, P. Electronic Structures, Vibrational Spectra, and Revised Assignment of Aniline and its Radical Cation: Theoretical Study. *J. Chem. Phys.* **2003,** *118*, 10900.
[29] Choe, J. C.; Cheong, N. R.; Park, S. M. Unimolecular Dissociation of Aniline Molecular Ion: A Theoretical Study. *Int. J. Mass Spectrom.* **2009,** *279*, 25–31.
[30] Pino, T.; Douin, S.; Boudin, N.; Bréchignac, Ph. Near Infrared Photodissociation Spectra of the Aniline+–Argon Ionic Complexes. *Chem. Phys. Lett.* **2006,** *419*, 356–361.
[31] Kato, K.; Yamanouchi, K. Photodecomposition Reaction of Trapped Aniline Cation by Photofragment Excitation Spectroscopy. *Chem. Phys. Lett.* **2004,** *397*, 237–241.
[32] Scarborough, T. D.; McAcy, C. J.; Beck, J.; Uiterwaal, C. J. G. J. Comparison of Ultrafast Intense-Field Photodynamics in Aniline and Nitrobenzene: Stability Under Amino and Nitro Substitution. *Phys. Chem. Chem. Phys.* **2019,** *21*, 6553-6558.
[33] Ledingham, K. W. D.; Singhal, R. P.; Smith, D. J.; McCanny, T.; Graham, P.; Kilic, H. S.; Peng, W. X.; Wang, S. L.; Langley, A. J.; Taday, P. F.; Kosmidis, C. Behavior of Polyatomic Molecules in Intense Infrared Laser Beams. *J. Phys. Chem. A.* **1998,** *102*, 3002-3005.
[34] Matsuda, A.; Fushitani, M.; Thomas, R. D.; Zhaunerchyk, V.; Hishikawa, A. Multiple Explosion Pathways of the Deuterated Benzene Trication in 9-fs Intense Laser Fields. *J. Phys. Chem. A.* **2009,** *113*, 2254-2260.
[35] Kitashoji, A.; Fujihara, A.; Yoshikawa, T.; Yatsuhashi, T. The Smallest Aromatic Tetracation Produced in Gas Phase by Intense Femtosecond Laser Pulses. *Chem. Lett.* **2019,** *48*, 1472-1475.
[36] Yatsuhashi, T.; Nakashima, N. Multiple Ionization and Coulomb Explosion of Molecules, Molecular Complexes, Clusters, and Solid Surfaces. *J. Photochem. Photobiol. C.* **2018,** *34*, 52-84.
[37] Tibbetts, K. M. Coherent Vibrational and Dissociation Dynamics of Polyatomic Radical Cations. *Chem. Eur. J.* **2019,** *25*, 8431-8439.
[38] Lezius, M.; Blanchet, V.; Yu, M.; Ivanov, Stolow, A. Polyatomic Molecules in Strong Laser Fields: Nonadiabatic Multielectron Dynamics. *J. Chem. Phys*. **2002,** *117*, 1575-1588.

[39] Bohinski, T.; Tibbetts, K. M.; Tarazkar, M.; Romanov, D.; Matsika, S.; Levis, R. J. Measurement of an Electronic Resonance in a Ground-State, Gas-Phase Acetophenone Cation via Strong-Field Mass Spectrometry. *J. Phys. Chem. Lett.* **2013,** *4*, 1587−1591.
[40] Bohinski, T.; Tibbetts, K. M.; Tarazkar, M.; Romanov, D.; Matsika, S.; Levis, R. J. Measurement of Ionic Resonances in Alkyl Phenyl Ketone Cations via Infrared Strong Field Mass Spectrometry, *J. Phys. Chem. A*, **2013,** *117*, 12374−12381.
[41] Gutsev, G. L.; Ampadu Boateng, D.; Jena, P.; Tibbetts, K. M. A Theoretical and Mass Spectrometry Study of Dimethyl Methylphosphonate: New Isomers and Cation Decay Channels in an Intense Femtosecond Laser Field. *J. Phys. Chem. A.* **2017,** *121*, 8414-8424.
[42] Hankin, S. M.; Villeneuve, D. M.; Corkum, P. B.; Rayner, D. M. Intense-Field Laser Ionization Rates in Atoms and Molecules. *Phys. Rev. A: At., Mol., Opt. Phys.* **2001,** *64*, 013405.
[43] Frisch, M. J.; Trucks, G. W.; Schlegel, H. B.; Scuseria, G. E.; Robb, M. A.; Cheeseman, J. R.; Scalmani, G.; Barone, V.; Mennucci, B.; Petersson, G. A, et al. *Gaussian 09*, Revision C.01, Gaussian, Inc., Wallingford CT, **2009**.
[44] Becke, A. D. Density-Functional Exchange-Energy Approximation with Correct Asymptotic Behavior. *Phys. Rev. A*. **1988,** *38*, 3098-3100.
[45] Perdew, J. P.; Wang, Y. Accurate and Simple Analytic Representation of the Electron-Gas Correlation Energy. *Phys. Rev. B*. **1992,** *45*, 13244-13249.
[46] Yang, K.; Zheng, J.; Zhao, Y.; Truhlar, D. G. Tests of the RPBE, revPBE, τ-HCTHhyb, ωB97X-D, and MOHLYP Density Functional Approximations and 29 Others Against Representative Databases for Diverse Bond Energies and Barrier Heights in Catalysis. *J. Chem. Phys*. **2010,** *132*, 164117.
[47] Stephens, P.J.; Devlin, F.J.; Chabalowski, C.F.N; Frisch, M.J. Ab Initio Calculation of Vibrational Absorption and Circular Dichroism Spectra Using Density Functional Force Fields. *J. Phys. Chem*. **1994**, *98*, 11623-11627
[48] Yanai, T.; Tew, D. P.; Handy, N. C. A new hybrid exchange–correlation functional using the Coulomb-attenuating method (CAM-B3LYP). *Chem. Phys. Lett*. **2004**, *393*, 51–57.
[49] Bartlett, R. J.; Musial, M. Coupled-Cluster Theory in Quantum Chemistry, Rev. Mod. Phys. 2007, **79**, 291-352.
[50] Ampadu Boateng, D.; Gutsev, G. L.; Jena, P.; Tibbetts, K. M. Dissociation Dynamics of 3- and 4-Nitrotoluene Radical Cations: Coherently Driven C–NO_2 Bond Homolysis. *J. Chem. Phys.* **2018,** *148*, 134305.
[51] Ampadu Boateng, D.; Word, M. D.; Gutsev, L. G.; Jena, P.; Tibbetts, K. M. Conserved Vibrational Coherence in the Ultrafast Rearrangement of 2-Nitrotoluene Radical Cation, *J. Phys. Chem. A.* **2019,** *123*, 1140 −1152.
[52] Weigend, F.; Ahlrichs, R. Balanced Basis Sets of Split Valence, Triple Zeta Valence and Quadruple Zeta Valence Quality for H to Rn: Design and Assessment of Accuracy. *Phys. Chem. Chem. Phys.* **2005,** *7*, 3297-3305.
[53] Reed, A. E.; Curtiss L. A.; Weinhold, F. Intermolecular Interactions from a Natural Bond Orbital, Donor-Acceptor Viewpoint. *Chem. Rev.* **1988,** *88*, 899-926.
[54] Gutman, I.; Potgieter, J. H. Isomers of Benzene. *J. Chem. Educ.* **1994,** *71*, 222-224.
[55] Krogh-Jespersen, K. Ab Initio Electronic Structure Calculations on the Benzene Dication and Other $C_6H_6^{2+}$ Isomers. *J. Am. Chem. Soc.* **1991,** *113*, 417-423.
[56] Rosi, M.; Bauschlicher, C. W. Jr.; Bakes, E. L. O. The Stability of $C_6H_6^{2+}$: The Implication for Polycyclic Aromatic Hydrocarbon Dications. *Astrophys. J.* **2004,** *609*, 1192–1196.
[57] Raczyńska, E. D.; Stępniewsk, T. M.; Kolczyńska, K. Consequence of One-Electron Oxidation and One-Electron Reduction for Aniline. *J. Mol. Model.* **2011,** *17*, 3229–3239.

[58] Gutsev, G. L.; Adamowicz, L. The Structure of the CF_4^- Anion and the Electron Affinity of the CF_4 Molecule. *J. Chem. Phys*. **1995,** *102,* 9309-9314.
[59] Gutsev, G. L.; Bartlett, R. J.; Compton, R. N. Electron Affinities of CO_2, OCS, and CS_2, *J. Chem. Phys*. **1998,** *108*, 6756-6762.
[60] Gutsev, G. L.; Rozyczko, P. B.; Bartlett, R. J.; Weatherford, C. A. Does N_2^- Exist? A Coupled-Cluster Study. *J. Chem. Phys*. **1999,** *110*, 5137-5139.
[61] Yatsuhashi, T.; Obayashi, T.; Tanaka, M.; Murakami, M.; Nakashima, N. Femtosecond Laser Ionization of Organic Amines with Very Low Ionization Potentials: Relatively Small Suppressed Ionization Features. *J. Phys. Chem. A*, **2006**, *110*, 7763-7771.
[62] Shimizu, S.; Kou, J.; Kawato, S.; Shimizu, K.; Sakabe, S.; Nakashima, N. Coulomb Explosion of Benzene Irradiated by an Intense Femtosecond Laser Pulse. *Chem. Phys. Lett.* **2000,** *317*, 609–614.
[63] Murakami, M.; Mizoguchi, R.; Shimada, Y.; Yatsuhashi, T.; Nakashima, N. Ionization and Fragmentation of Anthracene with an Intense Femtosecond Laser Pulse at 1.4 μm. *Chem. Phys. Lett.* **2005,** *403*, 238–241.
[64] Kaziannis, S.; Kosmidis, C. Comparative Study of Multielectron Ionization of Alkyl Halides Induced by Picosecond Laser Irradiation. *J. Phys. Chem. A*. **2007,** *111*, 2839-2851.
[65] Tibbetts, K. M.; Xing, X.; Rabitz, H. Systematic Trends in Photonic Reagent Induced Reactions in a Homologous Chemical Family. *J. Phys. Chem. A*, **2013,** *117*, 8205−8215.
[66] Yatsuhashi, T.; Nakashima, N. Dissociation and Multiply Charged Silicon Ejection in High Abundance from Hexamethyldisilane. *J. Phys. Chem. A*, **2010**, *114*, 11890-11895
[67] Krems, M.; Zirbel, J; Thomason, M; DuBois, R.D. Channel Electron Multiplier and Channelplate Efficiencies for Detecting Positive Ions. *Rev. Sci. Instrum.* **2005**, *76*, 093305

TOC Graphic